Ultrafast photo-induced dynamics of V2O3 thin films under hydrostatic pressure

Gaël Privault, Guénolé Huitric, Marius Hervé, Elzbieta Trzop, Julien Tranchant, Benoit Corraze, Zohra Khaldi, Laurent Cario, Etienne Janod, Jean-Claude Ameline, et al.

Ultrafast Photo-Induced Dynamics of V_2O_3 thin films under hydrostatic pressure

Gaël Privault[1], Guénolé Huitric[1], Marius Hervé[1], Elzbieta Trzop[1], Julien Tranchant[2], Benoit Corraze[2], Zohra Khaldi[2], Laurent Cario[2], Etienne Janod[2], Jean-Claude Ameline[1], Nicolas Godin[1] and Roman Bertoni[1,3*]

[1*]Univ Rennes, CNRS, IPR (Institut de Physique de Rennes), UMR 6251, Rennes, F-35000, France.

[2]Nantes Université, CNRS, Institut des Matériaux de Nantes Jean Rouxel, IMN, Nantes, F-44322, France.

[3]Dynamical Control of Materials Laboratory, CNRS-University of Rennes 1-University of Tokyo-International Research Laboratory.

*Corresponding author(s). E-mail(s): roman.bertoni@univ-rennes1.fr;

Abstract

Controlling material properties with light pulses represents one of the next great challenge in material science. To achieve this goal, one needs to impact the material on the relevant time scale for controlling electronic and phononic properties. Targeting this challenge becomes possible thanks to the emerging field of photo-induced phase transition when a femtosecond light pulse interacts with the system. Along this line, we demonstrate the possibility to perform femtosecond optical spectroscopy under control thermodynamical environment. This new experimental setup includes a very precise pressure control between 1 and 6 kbar. These experimental results clearly demonstrate an effect of hydrostatic pressure onto the out-of-equilibrium photo-response of V_2O_3. The main feature is a blue shift of the Brillouin frequency that correlates with an increasing speed of sound.

Keywords: Ultrafast Spectroscopy, Photo-Induced Phenomena, Thermo-Elastic effects

1 Introduction

Nowadays, a new field of research is related to the ability of controlling the functionality of materials by using intense external field. Indeed, the next challenge is not only to observe and to understand physical processes leading to the emergence of interesting properties in materials (magnetism, conductivity, etc) but to directly control the desired functions in the fastest and most efficient way. From that perspective, the current availability of ultrafast intense laser pulses has created a pivotal change in the last decades. It is indeed possible to act on the different degrees of freedom (spins, orbital, lattice and electrons) using electromagnetic waves covering a broad range of energy. Moreover, thanks to femtosecond laser pulses, the light-matter interaction may occur at the relevant time scale and induce nonthermal distributions. Such concept is extensively developed in the field of photo-induced phase transition where an intense light pulse is used to generate new phases such as photo-induced superconductivity

[1, 2], spin transition states [3, 4] or even "hidden phase" [5]. Those ultrashort light pulses are also relevant to investigate fundamental couplings in condensed matter such as electron-electron [6–8] or electron-phonon [9–12].
When dealing with Photo-Induced Phase Transition (PIPT), the temperature is very often the only external thermodynamical parameter used to explore the phase diagram of materials. This severely restricts the attainable area in the phase diagram and prevents thorough investigation of photo-induced dynamics near transition lines. From that perspective, the complementary use of hydrostatic pressure opens interesting new perspectives related to understanding of non equilibrium dynamics near critical end points in phase diagram.

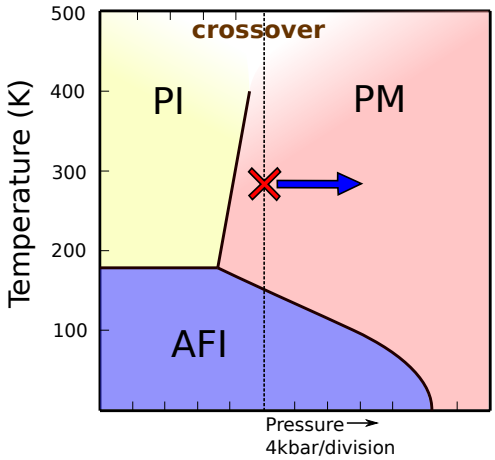

Fig. 1 Schematic phase diagram of V_2O_3. Red cross denotes the ambient thermodynamical conditions. Blue arrow illustates the expected displacement over the phase diagram.

V_2O_3 is a system often referred to as prototypical Mott material displaying a metal to insulator transition (MIT) (Figure 1)[13–15]. Under ambient conditions with a small amount of chromium used for chemical substitution, the material is in the paramagnetic insulating phase (PI) with an electronic gap of hundreds of meV. By applying pressure, the system enters in the paramagnetic correlated metallic phase (PM) as the electronic bandwidth is modulated and the electronic gap collapse. In this system, an antiferromagnetic phase (AFI) is present at low temperature with a transition temperature around 150 K at ambient pressure. According to the phase diagram of V_2O_3, one does not expect to cross any transition lines by applying pressure on pure V_2O_3. The system is indeed in the PM phase under ambient conditions and the application of hydrostatic pressure only drives the system further in the PM phase. Nevertheless, the application of hydrostatic pressure may be reflected in the out-of-equilibrium response of the material after photo-excitation. By using ultrafast pump-probe measurements, it is possible to follow the dynamics induced by femtosecond optical excitation on the relevant time scale. From that aspect, broadband optical spectroscopy is a useful tool that may provide valuable information regarding the complex out-of-equilibrium dynamics generated by femtosecond optical excitation[16].

2 Results

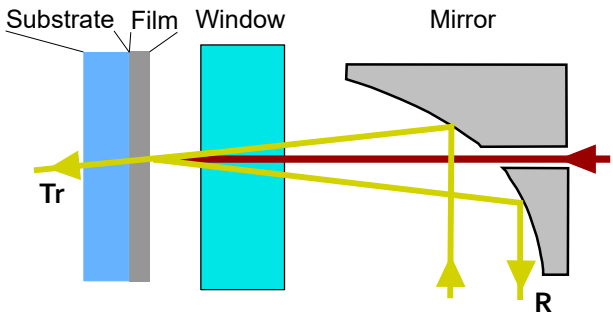

Fig. 2 Sketch of the experiment. Pump and probe beams are represented in dark red and khaki respectively. Both transmitted (Tr) and reflected (R) beam can be collected for measurement.

Here, we report the transient evolution of optical properties of a thin film of V_2O_3 after ultrafast photo-excitation by femtosecond laser pulses. The experimental observables are made of broadband optical spectra (450-725 nm) measured in two configurations: reflectivity and transmission (Figure 2). Both pump and probes beams arrive onto the film in quasi-normal incidence (less than 4°) after passing via a hollowed parabolic mirror. The thin film is sandwidched by the optical saphirre window and the substrate (0.5 mm thick). The sapphire window and the thin film are not perfectly parallel so reflected beams can be spatially separated. The pump laser energy is set to 1.55

eV (800 nm) with an estimated penetration depth of about $\sim$ 90 nm [17] while the film thickness is approximatively 190 $\mp$ 10 nm.

2.1 Ambient pressure measurements

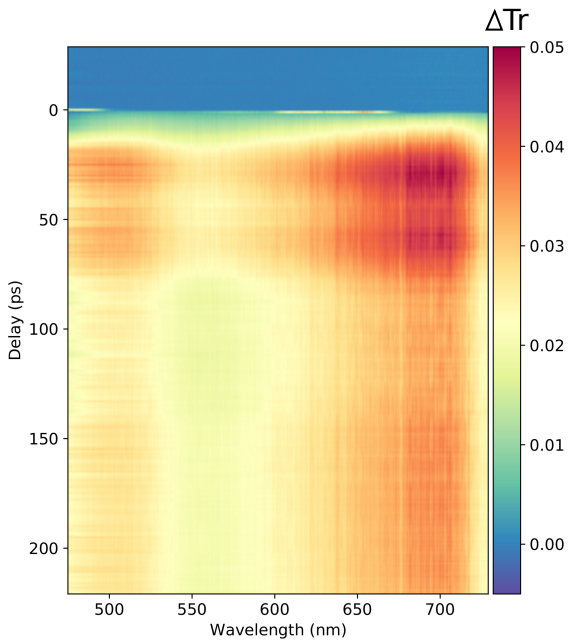

Fig. 3 Transient transmission of V_2O_3 thin film after photo-excitation with 800 nm pump under ambient pressure

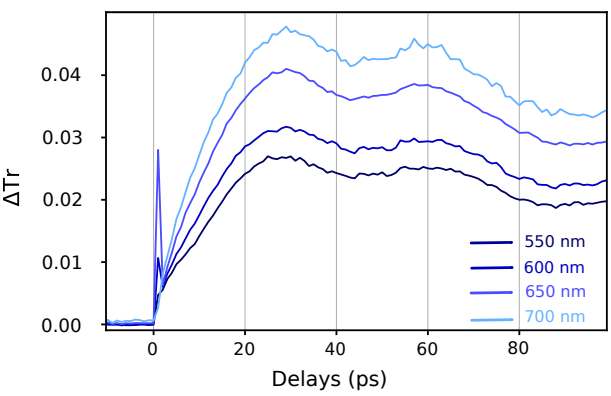

Fig. 4 Transient transmission of V_2O_3 thin film after 800 nm excitation at selected wavelengths under ambient pressure

The first step of this study is to perform ultrafast optical spectroscopy in the pressure cell at ambient pressure (1 bar) while the material is already surrounded by helium gas.

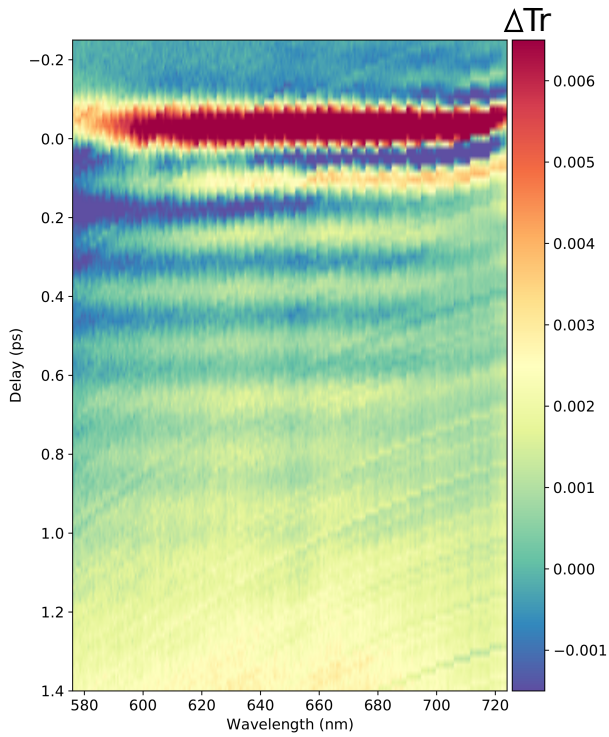

Fig. 5 Transient transmission of V_2O_3 thin film after 800 nm excitation on sub-picosecond timescale under ambient pressure

The transient transmission data obtained at ambient pressure is shown in figure 3. Photo-induced transient changes over the visible spectra last more than two hundreds of picoseconds. By slicing the spectrum at given wavelengths, one can observe more clearly the ongoing photo-induced dynamics (Figure 4). First, an instantaneous peak occurs around time zero where pump and probe overlap in the time domain. This ultrashort response relaxes very quickly. Such a feature can be ascribed to a mixture of ultrafast electronic response [18] and non-linear optical effects [19] induced by the intense electric field of the pump in the transparent sapphire windows. Consequently, a thorough investigation of those early dynamics often related to electron-electron dynamics is difficult in this experimental configuration. Afterwards, the transmission increases up to $\sim$ 30 ps for all probed wavelengths. After passing this maximum, the signal undergoes an oscillating behaviour before reaching a plateau around $\sim$ 100

ps. By looking at different wavelengths (Figure 4), one can observe that only the amplitude of signals changes but the overall photo-induced dynamics remain similar.

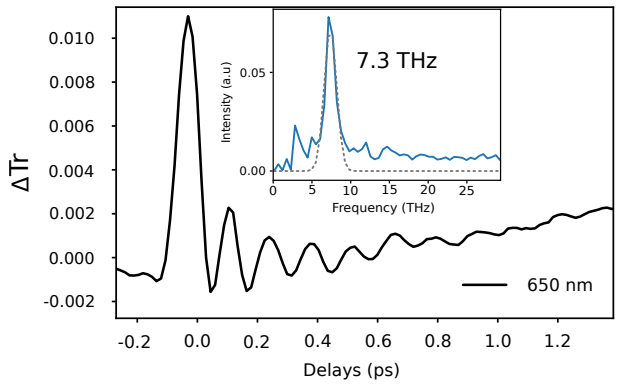

Fig. 6 Transient transmission of V_2O_3 on sub-picosecond at 650 nm. inset) FFT of the oscillating signal

Figure 5 displays transient spectrum related to the sub-picosecond dynamics observed at ambient pressure. This data set present a chirp correction that sets a proper timing for all wavelengths as explained in the section 4. A clear oscillating component modulating the full spectrum is observed and last for more than one picosecond. It is better seen when looking at a single wavelength dynamic around 650 nm (Figure 6). The frequency analysis of these oscillations indicates a single component centred around 7.3 THz (inset of Figure 6).

The transient reflectivity data are shown in figure 7. A small ultrashort peak lasting less than 1 ps around time zero is present for some wavelengths with the same physical origin than the one observed in transmission geometry. After, the different dynamics are observed with an initial negative signal for all wavelengths during the first tens of picoseconds. Later, a slower oscillating signal appears with an average value that differs depending on the wavelength (Figure 8). Nevertheless, similar to the transmission case, this slow oscillating behaviour occuring after 40 ps seems to be rather unaffected by the probing wavelength. This measurement in reflection geometry is very sensitive to acoustic effects and propagation of strain wave[20, 21]. It is sometimes referred to as time-resolved Brillouin scattering (TRBS)[22].

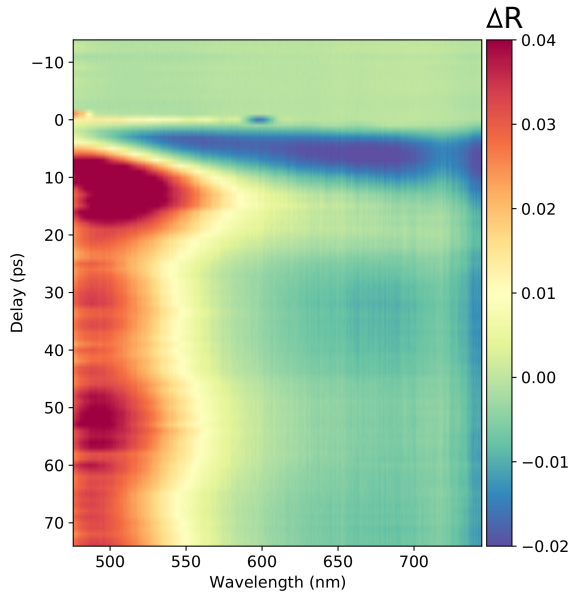

Fig. 7 Transient reflection of V_2O_3 thin film after photo-excitation with 800 nm pump

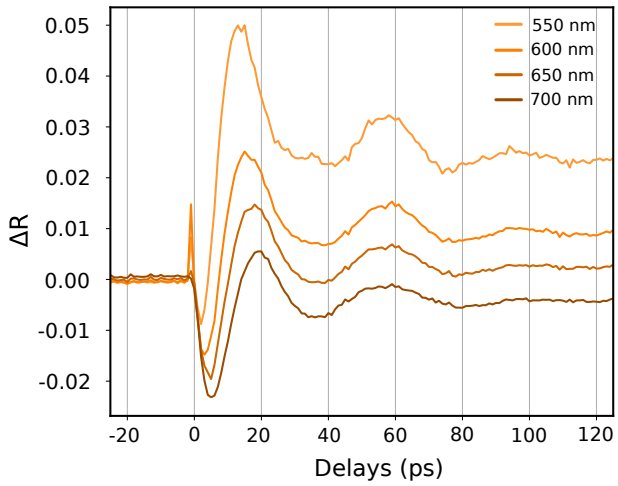

Fig. 8 Transient reflectivity of V_2O_3 thin film after 800 nm excitation at selected wavelengths under ambient pressure

2.2 High pressure measurements

In order to look for the impact of hydrostatic pressure onto the photo-induced dynamics, ultrafast measurements are performed under a hydrostatic pressure of 6 kbar. All other experimental parameters remain similar compared to the ambient pressure case. Figures 9 and 10 represent respectively the transient reflectivity and transmission in the very same fashion that the one presented

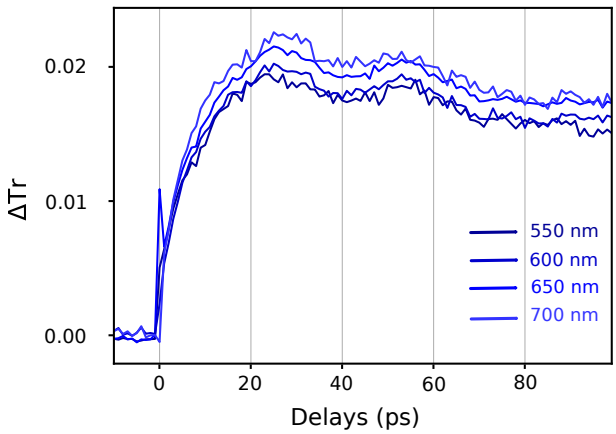

Fig. 9 Transient transmission of V_2O_3 thin film after 800 nm excitation at selected wavelengths under 6 kbar

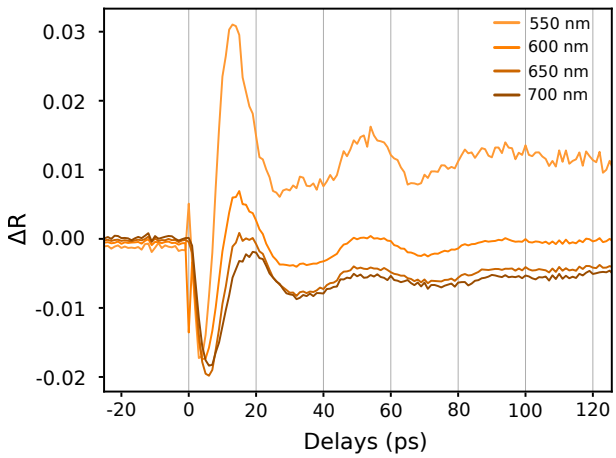

Fig. 10 Transient reflectivity of V_2O_3 thin film after 800 nm excitation at selected wavelengths under 6 kbar

for ambient pressure. One can see the dynamics in both geometries are very similar to those observed at ambient pressure. The transmission data reveals a transient increase of signal up to $\sim$ 20 ps followed by a small oscillating pattern. The transient signal reach a plateau after 80 ps. The transient reflectivity data set presents a negative signal lasting tens of picoseconds followed by an oscillating pattern around a mean value. In general, both signals follow the same trends pointing out that the very same photo-induced effects are generated in the high pressure case.

3 Discussion

The material being in the high temperature PM phase, the interaction between the optical pump pulse and V_2O_3 results in photo-excitation of electrons generating an excited electronic gas within the pump pulse duration (60 fs). First, the electronic subsystem is going to thermalize on sub-picosecond time-scale to reach a Fermi-Dirac statistical distribution [7, 18, 23]. Then, it interacts with the lattice through electron-phonon coupling in order to attain a thermal distribution in both the electronic and phononic subsystems. This exchange energy process should occurs on few to tens picosecond time-scale depending on the materials [9, 10, 12, 18] and is often modeled by a two- or multi-temperature model[24]. Nevertheless, it does not imply that the lattice has truly reached a thermal distribution[25]. The resulting effect is an ultrafast lattice heating with an in depth profile matching the optical penetration depth of the pump pulse. This process results in the generation of strain waves along the film thickness that affect the refractive index of the material[26]. The resulting dynamics already reported in several materials belongs to the class of photo-induced thermo-elastic effects that can be probed through optical spectroscopy [21, 26–29] or X-ray diffraction [30–32]. Despite being already few decades old and starting with the seminal work of Thomsen [20], this field of research is still vivid thanks to the development of new laser and X-ray sources and apparition of new techniques. The penetration depth profile of the

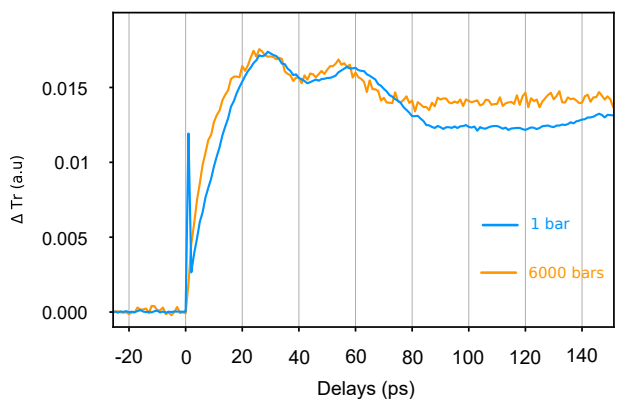

Fig. 11 Comparison of the transient transmission at 650 nm between 1 bar and 6 kbar

pump being smaller than the thickness of the film, it induces a multi-step dynamics in the probed acoustic time-scale. First, a strain wave launched from the film surface will propagate through the

full thickness of the film leading to a modulation of the measured transmission. The rising time from the maximum of transmission changes occurs around $\sim$ 26.5 ps at ambient pressure and $\sim$ 25 ps at 6 kbar. Considering this signal originating from the generation and travelling of elastic waves through the sample thickness, one can estimate the experimental agreement with the speed of sound previously reported in V_2O_3. The actual measurement leads to a value of $V_s = \frac{Lenght}{time} = \frac{190.10^{-9}}{26.5\times10^{-12}} = 7.15/km.s^{-1}$ in agreement with the value of $7.3/km.s^{-1}$ reported in literature for ambient pressure[33]. The slight shift towards earlier value ($\sim$ 25 ps) in the high pressure case support a modification of the speed of sound in the material with an estimated value of $\sim 7.6/km.s^{-1}$. This small but detectable shift is better seen in figure 11 where both transmission signals are directly normalized and compared. Also, the absence of clear wavelength dependence in the observed signals (Figure 4 and 8) independently of the applied pressure rules out the effect of time-resolved Brillouin scattering as been responsible for the oscillating behaviour observed up to 100 ps. Much likely, this effect is related to the travelling back and forth of strain waves inside the thin film that may be affected by the acoustic impedance with the substrate. Those oscillations are call acoustic eigen-modes in case of free standing films [26, 27]. The plateau lasting for hundreds of picoseconds afterwards is related to the deformation of the thin film induced by laser heating that will relax on longer time-scale via heat diffusion and energy exchange with the substrate.

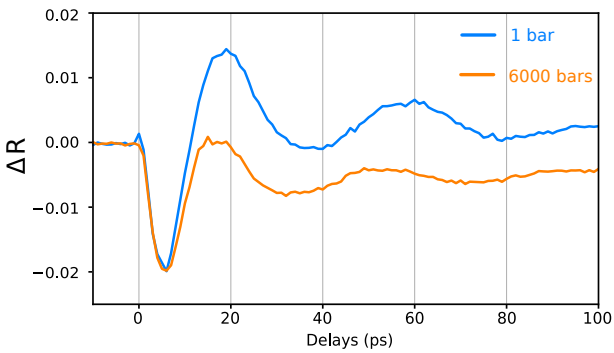

Fig. 12 Comparison of transient reflectivity at 650 nm between 1 bar and 6 kbar

The reflectivity measurements show different behaviours than the ones observed in transmission despite originating from the same photo-induced effects. The first negative signal directly comes from interferences phenomena between the pulse reflected from the surface and the one partially reflected by the strain wave propagating into the material. This effect, in the case of semi-infinite material, is refer as time domain Brillouin scattering [20, 34]. It also explains the strong wavelength dependency expected for TRBS[22] and observed within the first 20 ps (Figures 8 and 10). Indeed, the first positive extremun is shifted from 19 to 14 ps when changing wavelengths from 700 to 550 nm at ambient pressure. On contrary, the latter oscillating component lasting up to hundreds of picoseconds does not exhibit a clear temporal shift while changing the probing wavelength. This apparent absence of temporal shift is an indication that the observed dynamic does not correspond to TRBS. It seems more close to the observation of acoustic eigen-modes of the film whose frequencies should by independent of the probing wavelength[27]. When comparing transient reflectivity observed under ambient and high pressure (Figure 12), similar conclusions than the ones made for transmission can be drawn. A blue shift of the oscillating feature is observed in the high pressure case suggesting a more rigid material with increased speed of sound. Those results point out that even a moderate pressure of 0.6 GPa is enough to modulate the thermo-elastic photo-response of a thin film of V_2O_3.

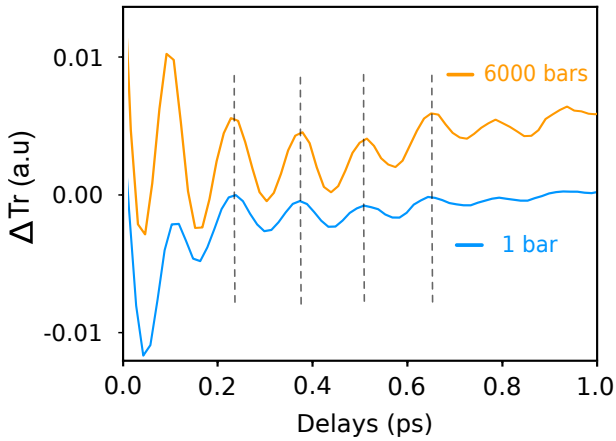

Fig. 13 Transient oscillating dynamics related to A_{1g} phonon at 1 bar and 6 kbar.

When looking at the sub-picosecond dynamics, oscillatory components are always present irrespective of the experimental geometry or the hydrostatic pressure (Figure 13). Both curves have been sligtly shifted for clarity. It reveals that the excited electronic gas preferentially coupled to the zone center fully symmetric A_{1g} optical mode to release excess energy. The measured value of 7.3 THz (Figure 6) matches the ones reported in previous experiments[18, 26, 35]. Under the investigated pressure range, no modification of the phonon frequency are observed as shown in figure 13, neither detectable variation of damping time. It implies that this phonon potential remains almost unperturbed within our sensitivity range up to 0.6 GPa which is expected for a rigid inorganic material such as V_2O_3.

4 Methods

4.1 Sample preparation

A thin film of pure V_2O_3 is deposited on a c-cut sapphire substrate by sputtering of a vanadium target in Ar discharge. Afterwards, the thin film is annealed at 530°C in a controlled atmosphere yielding in a single phased V_2O_3 layer. The thickness of 190 ± 10 nm is estimated via scanning electronic microscopy.

4.2 Optical measurements

All the results of this study are based on the classical pump-probe method. An intense ultra-short light pulse at a given photon energy is used to photo-excite the system (pump) while a second one of lower intensity (probe) is used to monitor the evolution of the system over time. The probing beam is made of a supercontiuum generated in a sapphire plate[36]. A typical spectrum is shown in the upper panel of figure 14. The spectral cut in the UV side comes both from the coupling between the probe pulse and the optical fibre used to bring the supercontinuum into the spectrometer and the drop of reflectivity of silver mirrors. The sharp edge in the IR side comes from a low pass filter used to remove noise from the pump pulse centered at 800 nm. We can also estimate the sensitivity of the setup by performing the analysis implemented for time-resolved data in the absence of pump pulse. The result is shown in the lower

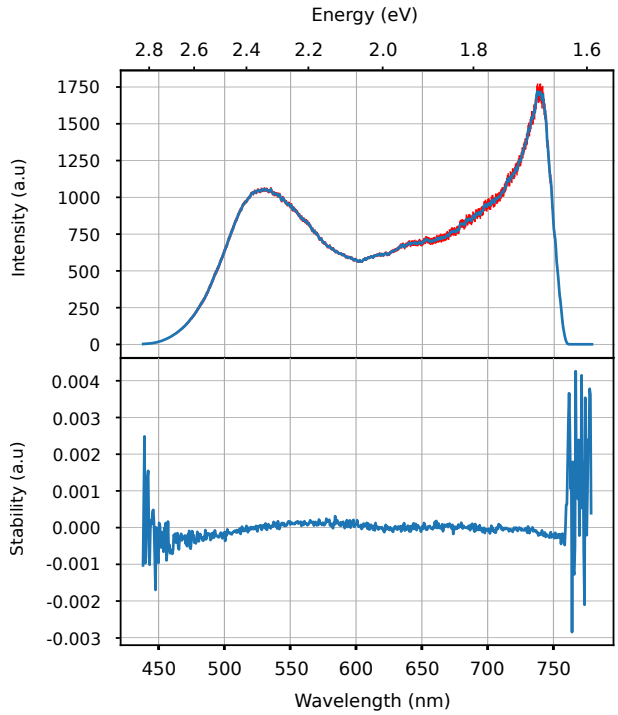

Fig. 14 Typical supercontinuum spectrum (top). Sensitivity of the optical setup (down).

panel of figure 14, displaying a global sensitivity of 2.10^{-4} (0.2 mOD) from 475 nm (2.6 eV) to 725 nm (1.7 eV). The pump photon energy is centred at 1.55 eV (800 nm) with an estimated duration of 60 fs. The typical size (FHWM) of the pump pulse of quasi-gaussian profile is around 160 μm leading to an average fluence of 50 μJ.mm^{-2}. This fluence is used for all experiments reported in this study. Each transient time-resolved spectra consists in an average of multiple single shots of excited or ground states. As the pump is chopped at half the laser frequency (500 Hz), alternative pump and unpumped spectra are measured by the camera. The spectra are sorted thanks to a small leak of the pump pulse onto the CDD camera that is used as a marker for excited spectrum. After, for each delay, 5000 shots of excited and unexcited spectrum are average and used to extract transients transmission and reflectivity. We define the transient transmission as the following:

$$\Delta T_R(t,\lambda) = \frac{T_R(t,\lambda) - T_R(off,\lambda)}{T_R(off,\lambda)} \qquad (1)$$

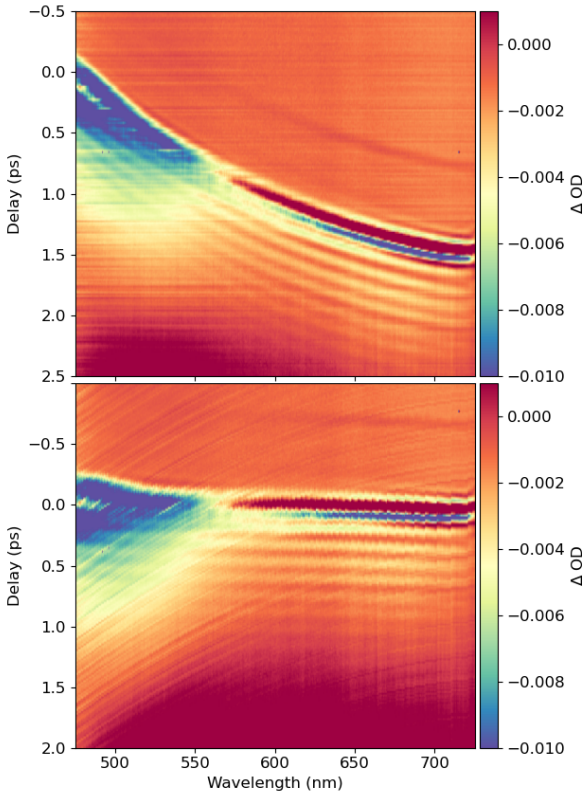

Fig. 15 Sub-picosecond data set without (top pannel) and with (lower pannel) chirp correction

Where $T_R(off, \lambda)$ corresponds to the transmission of the unperturbed material and $T_R(t, \lambda)$ to the one at a given time delay (t) after the photo-excitation. In the same way, the transient reflectivity in function of time is defined as followed:

$$\Delta R(t, \lambda) = \frac{R(t, \lambda) - R(off, \lambda)}{R(off, \lambda)}. \qquad (2)$$

Where $R(t, \lambda)$ is the reflectivity of excited states and $R(off, \lambda)$ the reflectivity of the unperturbed ground state. Those two quantities are the ones used to monitor the evolution of the material after ultrafast photo-excitation.

For very short delays, we may correct the data set for the chirp experienced by the probe beam. This effect arises from the ground velocity dispersion experienced by the probe beam and implies that each wavelength creates its own timing referential. Nevertheless, if the spectral resolution is sufficient, the main limitation for the experimental time resolution comes from the pump pulse duration [37]. This is illustrated by the figure 15 showing chirp uncorrected and corrected data set where the A_{1g} optical phonon of V_2O_3 is clearly visible in both cases despite the 1.25 ps duration of supercontinuum pulse in the probed range. It emphasises that all photo-induced informations are already embedded in data sets without chirp correction.

4.3 High pressure gas cell

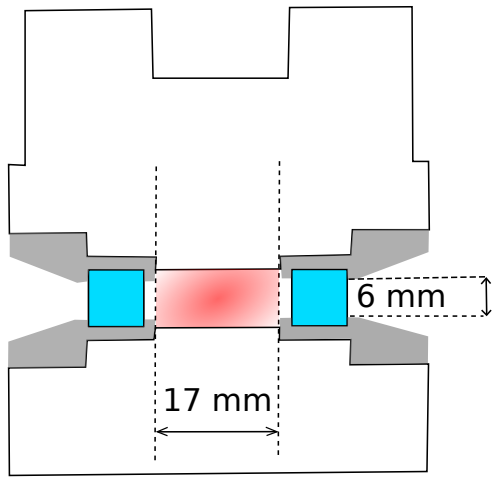

Fig. 16 Transverse cut of the pressure gas cell with relevant dimensions. The two sapphhire windows are shown in blue. The shaded red space denotes the sample area.

The complete high pressure setup is built on a multi-stages amplification process. First, a conventional gas compressor is used to pressurize the entire setup up to 1000 bars. Secondly, the primary stage is isolated and a piston-based compression is used to boost up the cell to 7 kbars. The high-pressure gas is delivered to the cell via a metallic capillary. A schematic transverse cut of the cell is drawn in figure 16. The pressure is monitored at the entrance of the capillary, in the primary stage. It allows for direct monitoring of the He gas pressure in-operando with precision of few bars. This is a substantial advantage over conventional diamond-like anvil cell relying on indirect measurement such as ruby fluorescence. The accuracy of the current apparatus is $\pm$ 10 bars (at 7 kbars) and $\pm$ 1 K in the operating range as

the cell fits into a home-made cryostat for cooling. It possesses two sapphire windows (Figure 16) used for both reflectivity and transmission optical measurements. The use of sapphire optical windows ensures good transmission in a spectral range spanning from 5 eV to 0.25 eV (250 to 5000 nm). The sample area, depicted in red, has a volume of 0.4 cm^3 allowing for the investigation of thin films as large as 5×5 mm^2. In addition, this gas cell apparatus, controlled by electro-valve, allows ramping and relaxing pressure with arbitrarily slow rate, as low as few bars per minute. This setup is especially relevant for the study of materials undergoing first order transition accompanied by significant volume changes. Indeed, a very slow variation is needed to accommodate the strain experienced by the material during the transition.

5 Conclusion

In conclusion, we demonstrate the ability to perform ultrafast optical spectroscopy in a high pressure He gas cell. The current setup is able to reach time resolution as good as ∼100 fs while conserving a signal to noise ratio of 10^{-4}. Using V_2O_3 as a benchmark material, the obtained results show a clear effect on the transient modulation of optical properties of a thin film of V_2O_3 mainly mediated by acoustic effects. Indeed, despite being a rigid inorganic material, clear modifications of dynamics induced by thermo-elastic effects are observed under the moderate pressure of 0.6 GPa. Nevertheless, we do not observed obvious modifications of the coherent optical A_{1g} mode suggesting only a small modification of the lattice potential under the investigated pressure. The possibility of very fine tuning of pressure could reflect on very accurate control of the photo-acoustic response of material. This capability is particularly relevant in the emerging field of photo-induced strain driven phenomena where the generation and control of strain wave could be used to induce phase transition [32]. Furthermore, this new experimental platform should be relevant for the study of soft correlated molecular materials where complete phase transition occurs within few kbars range allowing a large exploration of phase diagram [38].

Acknowledgments. Authors acknowledge Agence Nationale de la Recherche (ANR) for funding undergrant, ANR-21-CE30-0011-01 CRITICLAS. This work was carried out in the frame of the International Laboratory, DYNACOM IRL University of Tokyo - CNRS - UR1.

Declarations

- The authors declare no conflict of interest.

References

[1] D. Fausti, R. Tobey, N. Dean, S. Kaiser, A. Dienst, M. C. Hoffmann, S. Pyon, T. Takayama, H. Takagi and A. Cavalleri, *Science*, 2011, **331**, 189–191.

[2] M. Buzzi, D. Nicoletti, S. Fava, G. Jotzu, K. Miyagawa, K. Kanoda, A. Henderson, T. Siegrist, J. Schlueter, M.-S. Nam *et al.*, *Physical review letters*, 2021, **127**, 197002.

[3] M. Lorenc, J. Hébert, N. Moisan, E. Trzop, M. Servol, M. Buron-Le Cointe, H. Cailleau, M. L. Boillot, E. Pontecorvo, M. Wulff, S. Koshihara and E. Collet, *Phys. Rev. Lett.*, 2009, **103**, 2–5.

[4] R. M. van der Veen, O.-H. Kwon, A. Tissot, A. Hauser and A. H. Zewail, *Nat Chem*, 2013, **5**, 395–402.

[5] A. Kogar, A. Zong, P. E. Dolgirev, X. Shen, J. Straquadine, Y.-Q. Bie, X. Wang, T. Rohwer, I. Tung, Y. Yang *et al.*, *Nature Physics*, 2020, **16**, 159–163.

[6] M. Obergfell and J. Demsar, *Phys. Rev. Lett.*, 2020, **124**, 037401.

[7] M. Bauer, A. Marienfeld and M. Aeschlimann, *Progress in Surface Science*, 2015, **90**, 319–376.

[8] B. Rethfeld, A. Kaiser, M. Vicanek and G. Simon, *Phys. Rev. B*, 2002, **65**, 214303.

[9] L. Waldecker, R. Bertoni, R. Ernstorfer and J. Vorberger, *Phys. Rev. X*, 2016, **6**, 021003.

[10] H. E. Elsayed-Ali, T. B. Norris, M. A. Pessot and G. A. Mourou, *Phys. Rev. Lett.*, 1987,

58, 1212–1215.

[11] M. Sentef, A. F. Kemper, B. Moritz, J. K. Freericks, Z.-X. Shen and T. P. Devereaux, *Phys. Rev. X*, 2013, **3**, 041033.

[12] T. Chase, M. Trigo, A. Reid, R. Li, T. Vecchione, X. Shen, S. Weathersby, R. Coffee, N. Hartmann, D. Reis *et al.*, *Applied Physics Letters*, 2016, **108**, 041909.

[13] N. F. Mott, *Proc. Phys. Soc. A*, 1949, **62**, 416–422.

[14] P. Hansmann, A. Toschi, G. Sangiovanni, T. Saha-Dasgupta, S. Lupi, M. Marsi and K. Held, *Mott–Hubbard transition in V2O3 revisited*, 2013.

[15] D. B. McWhan, A. Menth, J. P. Remeika, W. F. Brinkman and T. M. Rice, *Phys. Rev. B*, 1973, **7**, 1920–1931.

[16] M. Maiuri, M. Garavelli and G. Cerullo, *Journal of the American Chemical Society*, 2019, **142**, 3–15.

[17] M. M. Qazilbash, A. Schafgans, K. Burch, S. Yun, B. Chae, B. Kim, H.-T. Kim and D. Basov, *Physical Review B*, 2008, **77**, 115121.

[18] G. Lantz, B. Mansart, D. Grieger, D. Boschetto, N. Nilforoushan, E. Papalazarou, N. Moisan, L. Perfetti, V. L. Jacques, D. Le Bolloc'h *et al.*, *Nature communications*, 2017, **8**, 1–7.

[19] M. Lorenc, M. Ziolek, R. Naskrecki, J. Karolczak, J. Kubicki and A. Maciejewski, *Applied Physics B*, 2002, **74**, 19–27.

[20] C. Thomsen, H. T. Grahn, H. J. Maris and J. Tauc, *Phys. Rev. B*, 1986, **34**, 4129–4138.

[21] B. Mansart, D. Boschetto, S. Sauvage, A. Rousse and M. Marsi, *EPL (Europhysics Letters)*, 2010, **92**, 37007.

[22] I. Chaban, H. D. Shin, C. Klieber, R. Busselez, V. E. Gusev, K. A. Nelson and T. Pezeril, *Review of Scientific Instruments*, 2017, **88**, 074904.

[23] R. Schoenlein, W. Lin, J. Fujimoto and G. Eesley, *Physical Review Letters*, 1987, **58**, 1680.

[24] S. Anisimov, B. Kapeliovich, T. Perelman *et al.*, *Zh. Eksp. Teor. Fiz*, 1974, **66**, 375–377.

[25] M. Trigo, J. Chen, V. Vishwanath, Y.-M. Sheu, T. Graber, R. Henning and D. Reis, *Physical Review B*, 2010, **82**, 235205.

[26] G. Huitric, M. Rodriguez-Fano, L. Gournay, N. Godin, M. Herve, G. Privault, J. Tranchant, Z. Khaldi, M. Cammarata, E. Collet *et al.*, *Faraday Discussions*, 2022.

[27] A. Levchuk, B. Wilk, G. Vaudel, F. Labb, B. Arnaud, K. Balin, J. Szade, P. Ruello and V. Juv, *Phys. Rev. B*, 2020, **101**, 180102.

[28] P. Ruello and V. E. Gusev, *Ultrasonics*, 2015, **56**, 21–35.

[29] O. Matsuda, M. C. Larciprete, R. L. Voti and O. B. Wright, *Ultrasonics*, 2015, **56**, 3–20.

[30] D. A. Reis, M. F. DeCamp, P. H. Bucksbaum, R. Clarke, E. Dufresne, M. Hertlein, R. Merlin, R. Falcone, H. Kapteyn, M. M. Murnane, J. Larsson, T. Missalla and J. S. Wark, *Phys. Rev. Lett.*, 2001, **86**, 3072–3075.

[31] D. Schick, M. Herzog, A. Bojahr, W. Leitenberger, A. Hertwig, R. Shayduk and M. Bargheer, *Structural Dynamics*, 2014, **1**, 064501.

[32] C. Mariette, M. Lorenc, H. Cailleau, E. Collet, L. Guérin, A. Volte, E. Trzop, R. Bertoni, X. Dong, B. Lépine *et al.*, *Nature communications*, 2021, **12**, 1–11.

[33] W. Yelon and J. Keem, *Solid State Communications*, 1979, **29**, 775–777.

[34] T. Parpiiev, M. Servol, M. Lorenc, I. Chaban, R. Lefort, E. Collet, H. Cailleau, P. Ruello, N. Daro, G. Chastanet *et al.*, *Applied Physics Letters*, 2017, **111**, 151901.

[35] D. Boschetto, M. Weis, J. Zhang, J. Caillaux, N. Nilforoushan, G. Lantz, B. Mansart, E. Papalazarou, N. Moisan, D. Grieger *et al.*,

Nature communications, 2019, **10**, 1–4.

[36] R. R. Alfano, *The supercontinuum laser source: fundamentals with updated references*, Springer, 2006.

[37] D. Polli, D. Brida, S. Mukamel, G. Lanzani and G. Cerullo, *Physical Review A*, 2010, **82**, 053809.

[38] D. Faltermeier, J. Barz, M. Dumm, M. Dressel, N. Drichko, B. Petrov, V. Semkin, R. Vlasova, C. Meźière and P. Batail, *Physical Review B*, 2007, **76**, 165113.